Journal of Colloid and Interface Science 575 (2020) 194–205

Contents lists available at ScienceDirect

Journal of Colloid and Interface Science

journal homepage: www.elsevier.com/locate/jcis

Adsorption of organic and inorganic arsenic from aqueous solutions using MgAl-LDH with incorporated nitroprusside

Gabriella Alexandre Borges [a], Gabriel Max Dias Ferreira [b], Kisla Prislen Félix Siqueira [c], Anderson Dias [a], Keirom Osmany Nàjera Navarro [b], Silvia Juliana Barros e Silva [b], Guilherme Dias Rodrigues [a], Aparecida Barbosa Mageste [b,*]

[a] Department of Chemistry, Federal University of Minas Gerais, Av. Antônio Carlos 6627, Campus Pampulha, 31270-901 Belo Horizonte, MG, Brazil
[b] Laboratory of Physical Chemistry and Environmental Chemistry, Department of Chemistry, Federal University of Ouro Preto (UFOP), Campus Morro do Cruzeiro, 35400-000 Ouro Preto, MG, Brazil
[c] Laboratory of Ceramic Materials and Raman Spectroscopy, Department of Chemistry, Federal University of Ouro Preto (UFOP), Campus Morro do Cruzeiro, 35400-000 Ouro Preto, MG, Brazil

GRAPHICAL ABSTRACT

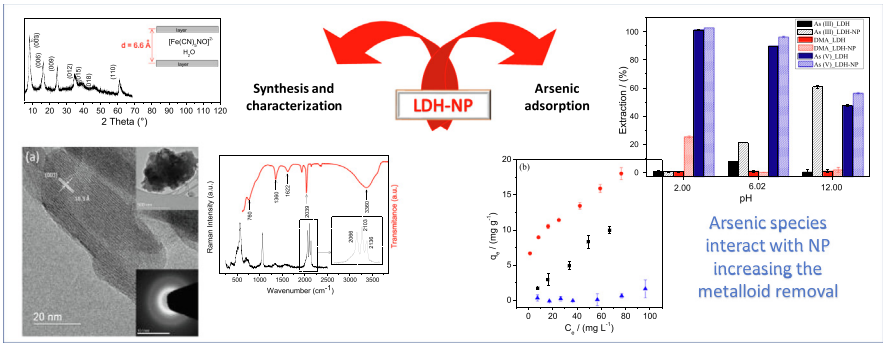

ARTICLE INFO

Article history:
Received 29 February 2020
Revised 11 April 2020
Accepted 19 April 2020
Available online 22 April 2020

Keywords:
Arsenic
Speciation
Adsorption
Layered double hydroxide
X-ray diffraction
Raman spectroscopy

ABSTRACT

An evaluation was made of the use of MgAl-LDH with incorporated nitroprusside as an adsorbent to remove inorganic arsenic (As(III) and As(V)) and organic arsenic (DMA) from aqueous matrices. The material was synthesized by the co-precipitation method at constant pH and was characterized by Raman spectroscopy, infrared spectroscopy, thermogravimetry, X-ray diffraction, and high-resolution transmission electron microscopy, before and after use in the adsorption process. The effects on adsorption of contact time, initial metalloid concentration, and pH were investigated. For an initial concentration of 10 mg L^{-1} and pH 2.00, the MgAl-LDH with incorporated nitroprusside was only able to adsorb the DMA and As (V) species, with removal percentages of 25.10 and 103.8%, respectively. At pH 6.02 and 12.00, only the inorganic species were adsorbed, with removal percentages of 22.93% and 60.07%, respectively, for As(III), and 89.81% and 71.64%, respectively, for As(V). Application of the Langmuir and Freundlich isotherm models indicated that the features of the adsorption process depended on the pH of the medium and

Abbreviations: LDH, layered double hydroxide; LDH-NP, layered double hydroxide with incorporated nitroprusside; q_e, equilibrium amount adsorbed; C_e, equilibrium concentration; WHO, World Health Organization; US EPA, United States Environmental Protection Agency; MMA, monomethylarsonic acid; DMA, dimethylarsinic acid; As (III), arsenious acid ions ($H_2AsO_3^-$, $HAsO_3^{2-}$, and AsO_3^{3-}); As (V), arsenic acid ions ($H_2AsO_4^-$, $HAsO_4^{2-}$, and AsO_4^{3-}); PZC, point of zero charge; %E, extraction percentage.

* Corresponding author.
E-mail address: aparecida.mageste@ufop.edu.br (A.B. Mageste).

https://doi.org/10.1016/j.jcis.2020.04.078

the arsenic species. The results showed that the use of MgAl-LDH with incorporated nitroprusside has potential for the development of techniques for the speciation of arsenic species.

1. Introduction

The contamination of water by arsenic is of global concern due to the serious human health problems that can be caused by long-term exposure to high levels of this metalloid, which can lead to the development of several types of cancer, cardiovascular and respiratory diseases, nervous system disorders, and diabetes [1]. Concentrations of total arsenic up to 5000 μg L^{-1} have been found in subterranean waters, greatly exceeding the value of 10 μg L^{-1} recommended by the World Health Organization (WHO) and the United States Environmental Protection Agency (US EPA) [2,3], which has the increased the concerns of health agencies worldwide.

Arsenic is found in nature in different chemical forms that have varying degrees of toxicity. Most commonly, arsenic is present as an oxyanion in inorganic compounds in the forms As(III) ($H_2AsO_3^-$, $HAsO_3^{2-}$, and AsO_3^{3-}) and As(V) ($H_2AsO_4^-$, $HAsO_4^{2-}$, and AsO_4^{3-}) [4], with the trivalent form being much more toxic than the pentavalent form [5]. In addition, there are organic forms of arsenic, such as monomethylarsonic acid (MMA) and dimethylarsinic acid (DMA), which are less toxic than the inorganic forms [6].

Research efforts have been devoted to the search for methods that can provide efficient removal of arsenic from water, as well as the development of techniques for speciation of the different forms of arsenic. In this context, adsorption processes are among the most efficient and widely used techniques for the removal of contaminants from water [7–12], mainly due to their low cost and ease of operation [2]. Various adsorbents have been proposed for the treatment of water containing arsenic, including cellulose derivatives, hydrogels, micro- and macro-porous resins, carbonaceous materials, red mud, lateritic soils, calcined bauxite, resins, clay minerals, and metal oxides and hydroxides [13–17]. Many of these adsorbents have limitations related to the difficulty of synthesis, low adsorption capacity, and risk of secondary pollution [3]. Consequently, there is continuing interest in the development of new materials for the adsorption of arsenic.

The use of layered double hydroxides (LDHs) to remove arsenic from water has emerged as an attractive option due to their hydrophilic nature and high anion exchange capacity [18]. LDHs, also known as anionic clays, are compounds analogous to brucite ($Mg(OH)_2$), with positively charged layers whose charges are counterbalanced by interlamellar, interchangeable, hydrated anions. The chemical structure of this class of compounds can be described by the general formula $[M^{2+}_{1-x}M^{3+}_x(OH)_2]A^{m-}_{x/m}.nH_2O$, where M^{2+} and M^{3+} are divalent and trivalent metal cations, A^{m-} is the intercalated anion with charge *m*-, and *x* is the $M^{3+}/(M^{3+} + M^{2+})$ ratio [4]. In this way, LDHs are versatile since they can be synthesized in a variety of combinations of cations and anions. In comparison with other conventional materials usually used in adsorption studies, LDHs present good thermal stability, have memory effect, and they can be synthesized relatively simply and cheaply [19,20]. In addition, the synthesis of LDHs is highly reproductible, which is fundamental from the point of view of industrial applications. Despite these advantages, the selectivity of LDHs can be low in front the oxyanion adsorption.

Hongtao et al. [21] evaluated the adsorption of As(V) on LDH of the type MgAlFe-LDH, finding that the adsorption of this arsenic species was affected by the pH of the medium and the chemical nature of the intercalated anion, with higher adsorption capacity achieved with the nitrate anion, compared to chloride. Lee et al. [2] obtained similar results for the effect of pH in the removal of As(V) using MgAl-LDH. In addition, it was found that the adsorption capacity increased from 19.7 mg g^{-1}, using non-calcined LDH, to 102.9 mg g^{-1}, using material calcined at 400 °C. More recently, Lee et al. [16] used CoAl-LDH on a boehmite surface to remove As(V) from aqueous matrices, achieving 100% removal of this species from a 2000 mg L^{-1} solution using an adsorbent concentration of 1.25 g L^{-1}, with As(V) becoming intercalated in the interlamellar region by means of ion exchange and complex formation. Despite advances in this area, data are scarce concerning the adsorption of other arsenic species using LDH. To the best of our knowledge, there has been only a single study evaluating the adsorption of As(III) [22], while no studies have considered the adsorption of organic arsenic.

In this work, evaluation was made of the use of LDH of the type MgAl-LDH, with incorporated nitroprusside ($[Fe(CN)_5NO]^{2-}$), denoted LDH-NP [23], as an adsorbent for different species of arsenic (As(III), As(V), and DMA), based on the high affinity of arsenic for species containing iron [24,25]. The material was characterized by Raman spectroscopy, infrared spectroscopy, thermogravimetry, and X-ray diffraction. Adsorption studies were performed using different contact times, initial metalloid concentrations, and pH of the medium.

2. Materials and methods

2.1. Reagents

Magnesium nitrate ($Mg(NO_3)_2{\cdot}6H_2O$; 99%), sodium arsenite ($AsNaO_2$; ≥99.0%), and cacodylic acid ($C_2H_7AsO_2$; ≥99.0%) were purchased from Sigma-Aldrich. Aluminum nitrate ($Al(NO_3)_3{\cdot}9H_2O$; 98.0%) and sodium nitroprusside ($Na_2[Fe(CN)_5NO]{\cdot}2H_2O$; 99.9%) were purchased from Vetec. Nitric acid (HNO_3; 65.0%) and sodium hydroxide (NaOH; 99.0%) were purchased from Synth. Hydrochloric acid (HCl; 37%) was purchased from Neon. Sodium arsenate ($Na_2HAsO_4{\cdot}7H_2O$; 98.0%) was purchased from Merck. All the reagents used in this study were of analytical grade and were utilized as received, without further purification. Deionized water was used to prepare all the solutions.

2.2. Synthesis of the materials

The conventional LDH, with nominal composition $Mg_4Al_2(OH)_{12}{\cdot}CO_3{\cdot}4H_2O$, was prepared using the co-precipitation method at constant pH [26]. Firstly, stoichiometric amounts of the reagents $Mg(NO_3)_2{\cdot}6H_2O$, $Al(NO_3)_3{\cdot}9H_2O$, NaOH, and Na_2CO_3 were separately solubilized in deionized water. Then, the solutions with the cations (Mg^{2+} and Al^{3+}) were slowly added to a reaction flask containing the Na_2CO_3 solution (1 mol·L^{-1}), where they were kept for 240 min, at 40 °C, under constant agitation. The pH of the system was maintained constant at 10 during all reaction time by the addition drop-by-drop of the NaOH solution (10 mol·L^{-1}). After that time, the system was allowed in a shaker-incubator with controlled temperature (TE-424, Tecnal) for 30 h at 55 °C. The resulting suspension was filtered, washed with deionized water, and dried in an oven at 50 °C. The material obtained was macerated and stored in desiccator until use.

The LDH with intercalated nitroprusside (LDH-NP), with nominal composition $Mg_4Al_2(OH)_{12}{\cdot}Fe(CN)_5NO{\cdot}4H_2O$, was also prepared by the co-precipitation method at constant pH, in a similar way as described above, following the stoichiometry of the following reaction:

$$4Mg(NO_3)_2 \cdot 6H_2O + 2Al(NO_3)_3 \cdot 9H_2O + 1Na_2[Fe(CN)_5NO] \cdot 2H_2O + 12NaOH \rightarrow Mg_4Al_2(OH)_{12} \cdot Fe(CN)_5NO \cdot 4H_2O + 14NaNO_3 + 13H_2O \quad (1)$$

Firstly, stoichiometric amounts of the reagents $Mg(NO_3)_2{\cdot}6H_2O$, $Al(NO_3)_3{\cdot}9H_2O$, NaOH, and $Na_2[Fe(CN)_5NO]{\cdot}2H_2O$ were individually solubilized in deionized water. The cation solutions were added dropwise to a reaction flask containing the nitroprusside solution (1 mol·L^{-1}), maintaining constant pH 10 by the addition of 10 mol L^{-1} NaOH solution. The mixture in the flask was kept at 40 °C, for 240 min, under constant agitation. After this period, the resulting mixture was submitted to thermal treatment at 55 °C for 24 h in a shaker-incubator. The solid material produced was filtered, washed with deionized water, dried in an oven at 50 °C, macerated, and stored in desiccator until use.

2.3. Characterization of the synthesized materials

The crystalline structures and the presence or absence of secondary phases in the synthesized materials were investigated by X-ray diffraction (XRD) measurements, using a PANalytical X'Pert3 diffractometer operating at 45 kV and 40 mA, with Cu Kα radiation, and scanning in the 2θ range 5–90°.

Morphological, chemical and structural features of the samples were investigated by transmission electron microscopy (TEM) and related techniques: selected-area electron diffraction (SAED), energy dispersive spectroscopy (EDS), and electron energy-loss spectroscopy (EELS). A reliable and versatile Tecnai G2-20 (FEI) transmission microscope was employed at 200 kV in powders dispersed in isopropanol and ultrasonicated for 15 min. Holey carbon-copper grids of #300 mesh were used as support for all the investigated samples.

Thermogravimetric analysis (DTA-TG) was performed using a Shimadzu DTG60 analyzer equipped with an alumina sample holder. The samples were heated from 30 to 600 °C, at a rate of 10 °C min^{-1}, in an atmosphere of N_2.

Infrared spectroscopy (FTIR) analyses were performed using an MB 3000 FTIR spectrometer (ABB Bomen, Quebec, Canada) operated in attenuated total reflection (ATR) mode. The spectra were acquired in the range from 500 to 4000 cm^{-1}.

Raman scattering data were collected in a Horiba Jobin-Yvon LABRAM HR spectrometer equipped with a Peltier-cooled CCD detector, and excitation source from a helium–neon laser (632.8 nm and power of 6 mW on the surface of the sample). An Olympus confocal microscope (100 × objective lens) was used for obtaining a typical experimental resolution of 1 cm^{-1} in 10 accumulations of 10 s. All resulting spectra were corrected using the Bose-Einstein thermal factor [27].

The point of zero charge (PZC) of the LDH-NP was obtained as follows [28]: 0.0250 g of the material was added to 25 mL of a 0.1 mol L^{-1} NaCl solution in deionized water, with the initial pH adjusted to 2.01, 4.00, 5.98, 8.08, 10.01, and 11.99. The pH adjustment was performed using solutions of HCl (0.1 or 1 mol L^{-1}) or NaOH (0.1 or 1 mol L^{-1}). The mixtures were then stirred for 24 h at 150 rpm and 25 °C, followed by collection of the supernatants for determination of the final pH. The difference between the final and initial pH values (ΔpH) was plotted against the initial pH and the PCZ was defined as the initial pH value at which ΔpH was zero. The experiments were performed in triplicate.

2.4. Adsorption experiments

2.4.1. Adsorption of different As species using the conventional LDH and LDH-NP

Initial arsenic adsorption tests were performed using the conventional LDH and LDH-NP. For this, 15.0 mL volumes of a 10.00 mg L^{-1} solution of arsenic (As(III), As(V), or DMA), with the pH adjusted to 2.00, 6.02, or 12.00, were added to 125 mL Erlenmeyer flasks containing 0.0200 g of the adsorbent (LDH or LDH-NP). The pH adjustment was performed using solutions of HCl (0.1 or 1 mol L^{-1}) or NaOH (0.1 or 1 mol L^{-1}). The systems obtained were agitated for 24 h, at 150 rpm and 25 °C, in a shaker-incubator with controlled temperature (TE-424, Tecnal). The samples were then collected and transferred to 50 mL centrifuge tubes, followed by centrifugation at 3000 rpm (Model 280, Excelsa 3, Fanem). The supernatant was then collected for analysis using Inductively Coupled Plasma Optical Emission Spectrometry (ICP-OES – Varian 725 ES). Systems without the presence of the arsenic species were prepared in the same way and used as blanks. The experiments were performed in duplicate.

The extraction percentages (%E) obtained for the arsenic species under each condition evaluated were calculated using Equation (2).

$$\%E = \frac{[As]_{initial} - [As]_{final}}{[As]_{initial}} x100 \quad (2)$$

where $[As]_{initial}$ and $[As]_{final}$ are the concentrations of the arsenic species in the supernatant before and after the adsorption process, respectively.

2.4.2. Adsorption isotherms

Adsorption isotherms for adsorption of the arsenic species investigated (As(III), As(V), and DMA) on LDH-NP were obtained at pH 2.00, 6.02, and 12.00. The experiments were similar to those described in Section 2.4.1, varying the initial concentrations of arsenic in the supernatant, as follows: 10, 20, 30, 40, 60, 80, and 100 mg L^{-1} for As(III) and DMA, and 10, 20, 30, 40, 60, 80, 100, 150, and 200 mg L^{-1} for As(V). The supernatants collected were suitably diluted prior to analysis using ICP-OES.

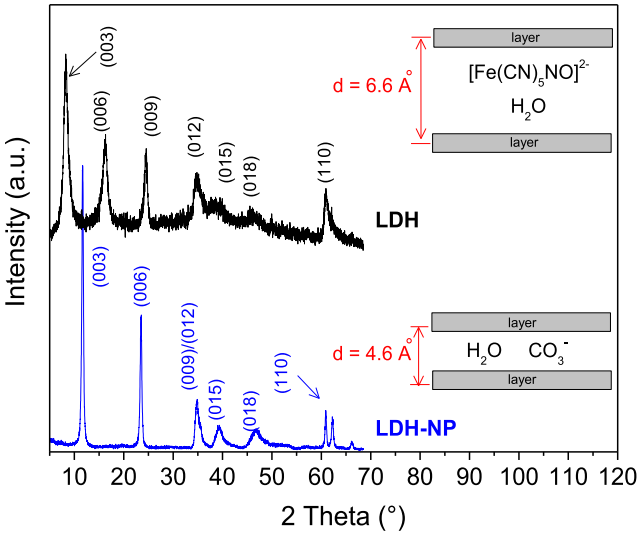

Fig. 1. XRD patterns for (a) LDH (blue line) and (b) LDH-NP (black line) materials. The crystalline planes were assigned according to ICDD card #51-1525. Schematic drawings emphasize the difference in the interlamellar spacing. (For interpretation of the references to colour in this figure legend, the reader is referred to the web version of this article.)

The amounts of the arsenic species adsorbed on LDH-NP (q_e) were calculated using Equation (3).

$$q_e = \frac{(C_o - C_e) \cdot V}{m} \quad (3)$$

where C_o and C_e are the initial and equilibrium concentrations in the supernatant, respectively, V is the total supernatant volume, and m is the mass of adsorbent. The experiments were performed in duplicate.

All pH values reported throughout the Sections 2.2 and 2.3 were the values measured in pH meter, respecting the significative digits.

2.4.3. Effect of contact time

Evaluation was made of the effect of the contact time on the adsorption of As(V) on LDH-NP. The experiments were performed as described in Section 2.4.1, using an arsenic solution with an initial concentration of 20 mg L^{-1}. The contact times used were 0.5, 1, 3, 5, 7, 9 12, 16, 20, and 24 h. The adsorbed amount at each time (q_t) was obtained by Equation (3), in which C_e was replaced with C_t, the arsenic concentration in the supernatant at time t. The experiments were performed in duplicate.

3. Results and discussion

3.1. Characterization of LDH and LDH-NP

Fig. 1 shows XRD data for the magnesium and aluminum layered double hydroxides intercalated with carbonate anions (LDH) and nitroprusside (LDH-NP).

The diffractograms confirmed the intercalation of nitroprusside, which caused a spacing increase of approximately 42%. After the intercalation, the basal space was around 6.6 Å, which is in accordance with the size of the anionic complex of the transition metal [23,29]. The materials exhibited diffraction patterns characteristic of the hydrotalcite structure, with sharp and symmetric reflections of the (0 0 3), (0 0 6), and (0 0 9) basal planes, and asymmetric reflections for the (0 1 2), (0 1 5), and (0 1 8) non-basal planes. The crystalline planes were assigned according to ICDD (International Centre for Diffraction Data) card #51–1525. Basal (00*l*) planes are related to the stacking of the layers. Non-basal (*hk*0) planes are associated with the organization of the structure inside the layers, while (0*kl*) planes are related to the ordering of one layer relative to an adjacent layer [30]. In the present case, it could be seen that there was a blue-shift of the basal planes, due to the intercalation of the nitroprusside.

The lattice parameters a and c were calculated as described by Pérez-Ramírez et al. [31] for a hexagonal unit cell, assuming 3R polytypism for the hydrotalcite. The value of the cell constant a is calculated as $a = 2d_{(1\,1\,0)}$ and corresponds to the average distance of the cations present within the layers of the LDH structure. The c parameter is related to the layer thickness and interlayer distance and is commonly calculated as $c = 3d_{(0\,0\,3)}$. However, it has been proposed that c can be better determined by averaging the positions of the diffraction peaks corresponding to the basal planes: $c = 3/2\{d_{(0\,0\,3)} + 2d_{(0\,0\,6)}\}$ or $c=\{d_{(0\,0\,3)} + 2d_{(0\,0\,6)} + 3d_{(0\,0\,9)}\}$ [31]. In the present case, the second formula was used, since the positions of all the basal planes were easily identified. The values for the lattice parameters and the basal spacing are provided in Table 1.

The $d_{(0\,0\,3)}$ interplanar spacing represents two lamellar layers and one interlamellar layer, provided with hydrated anions. On the other hand, the $d_{(0\,0\,6)}$ distance refers to the lamellar layer consisting of divalent cations, trivalent cations, and oxygen. The values found for the LDH-NP were very close to those reported by Boclair et al. [29] and Taylor et al. [32], who obtained values of 11.09 and 11.0, respectively, for $d_{(0\,0\,3)}$, and 5.57 and 5.47, respectively, for $d_{(0\,0\,6)}$. The basal spacing (d) was calculated by the Bragg equation, using the average: $1/3(d_{(0\,0\,3)} + d_{(0\,0\,6)} + d_{(0\,0\,9)})$. The basal spacing values (Table 1) are consistent with the size of nitroprusside anions, indicating the intercalation of the complex [23,29]. The average crystallite size was determined by the Scherrer method, considering the average size between the first two well-defined peaks, either (0 0 3) or (0 0 6) [31]. The results showed that the calculated particle size of LDH-NP (8 nm) was lower than that of the conventional LDH (23 nm) (Table 1). Smaller particles imply greater peak widths, which in turn reflect less crystalline materials. Therefore, the values obtained are in accordance with the XRD results.

The results obtained from TEM analysis of the LDH-NP samples are presented in Fig. 2. Morphological features are presented as low-magnification and high-resolution TEM images, while structural characteristics of the LDH-NP samples are exhibited as SAED patterns. The morphology of the samples shows nanometer-sized platelets formed by agglomerated smaller particles (Fig. 2a, inset: top right). High-resolution TEM image (Fig. 2) shows dominating interplanar spacings of the order of 10.3 Å, which can be related to the (0 0 3) planes of the rhombohedral ($R\bar{3}m$) space group, in agreement with the XRD data (Table 1). The polycrystalline character of the synthesized materials was verified by the SAED pattern (Fig. 2a, inset: bottom right), where only diffuse rings can be visualized. Chemical characteristics of the LDH-NP materials are presented in Fig. 2b. In this Figure, EDS/EELS spectra reveal both the valence electron (low-loss) peaks and the ionization edges of the fine structure of the materials. It was possible to observe and attribute many spectral features, corresponding to different excitation processes, thus corroborating the high purity of the samples. EDS spectrum evidenced the presence of Mg, Al, O, and Fe (Cu lines are due to the TEM grids), while EELS spectrum detected the presence of C, N, O, and Fe ions, as expected for chemically pure samples.

In addition to XRD and TEM, spectroscopic techniques were used to provide evidence of the insertion of anion complexes into the LDH. The FTIR and Raman spectra of LDH-NP are shown in Fig. 3. According to the literature, the insertion of cyanide-containing anions and complexes into LDH is easily demonstrated by the appearance of ν(CN) vibrations in the 2200–2000 cm^{-1} region of the infrared spectrum of the material [29]. A broad band at around 3360 cm^{-1} was related to stretching vibrations of the OH groups in the brucite-like layer [23,29]. A band at 2039 cm^{-1} could be attributed to CN stretching, while a band at 1622 cm^{-1} could be attributed to NO and OH stretching [23,29]. According to da Silva et al. [23], the presence of a strong band at 2039 cm^{-1} for intercalated materials is due to replacement of the NO ligand by water

Table 1
Lattice parameters, basal spacings, and crystallite sizes for the synthesized LDH materials.

Samples	Interplanar distance (Å)			Basal spacing (Å)	Lattice parameter (Å)		Crystallite size (nm)
	d_{003}	d_{006}	d_{009}		a	c	
LDH	7.57	3.78	2.57	4.64	3.04	22.84	23
LDH-NP	10.65	5.43	3.62	6.57	3.04	32.37	8

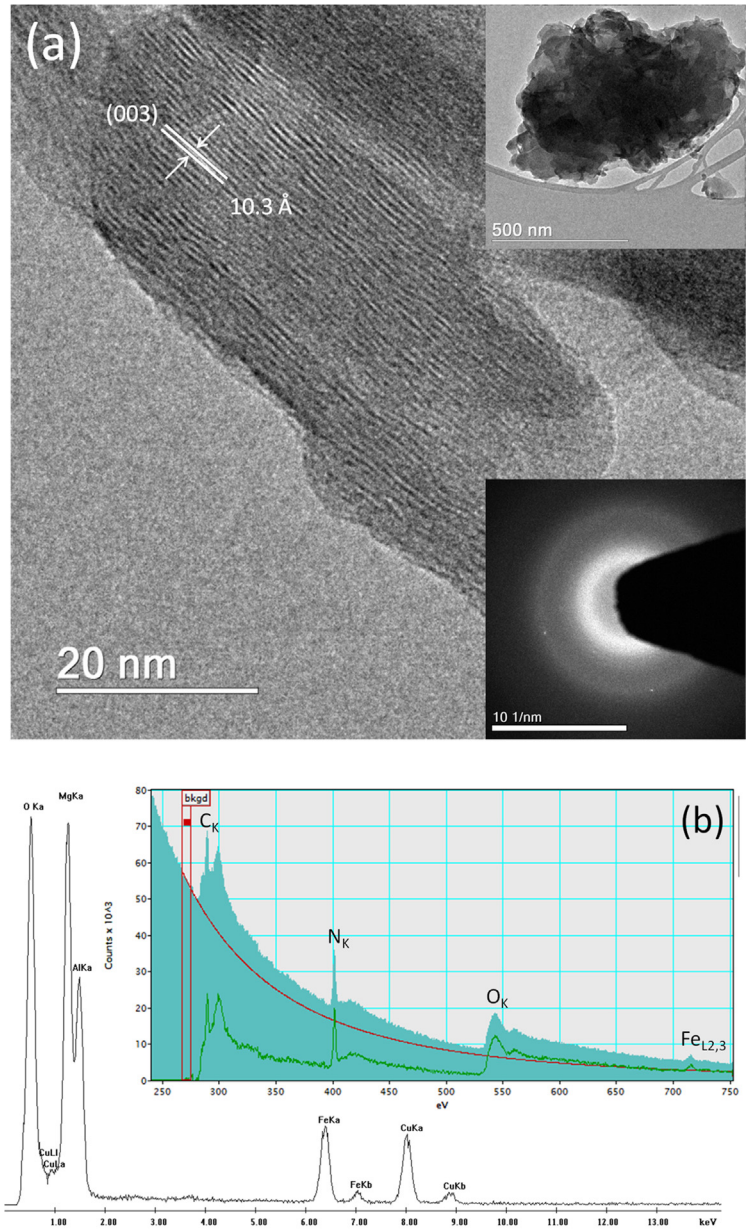

Fig. 2. (a) High-resolution TEM image for the LDH-NP materials with interplanar spacings of 10.3 Å, which are related to the (0 0 3) planes of the rhombohedral ($R\bar{3}m$) structure. Inset: low-magnification TEM image (top right) and SAED pattern (bottom right) evidencing the polycrystalline character of the sample; (b) EDS/EELS spectra with the electronic energies of the ions present into the structure: Mg, Al and Fe signals are shown in the EDS spectrum, while C, N, O, and Fe signals are shown in the EELS spectrum.

molecules, forming $[Fe(CN)_5H_2O]^{3-}$, while bands at around 1360 cm^{-1} are related to carbonate. In addition, a weak band at 760 cm^{-1} could be assigned to Fe–N stretching and Fe—N—O bending [33].

The Raman spectrum of LDH-NP was consistent with its crystalline structure and chemical composition. The hydrotalcite structure is rhombohedral ($R\bar{3}m$, Z = 3) and the Raman spectra for different compositions have been described in detail by Bellotto et al. [34] and Richardson et al. [35]. However, according to Vieira et al. [36], the number of modes observed in the spectra for LDH-like materials are fewer than expected from the Wyckoff sites of all atoms of the unit cell. This is because these materials can exhibit very disordered structures, which can lead to deviation from the selection rules and the activation of prohibited modes in Raman spectroscopy (the same is true for infrared spectroscopy) [36]. Therefore, the present analysis was based on the main Raman modes observed for LDH materials and nitroprusside anions. It should be noted that, to the best of our knowledge, this is the first study to present the Raman spectrum for LDH with intercalated nitroprusside.

The Raman spectrum was collected in the region from 250 to 2500 cm^{-1}, at room temperature. A band at 562 cm^{-1} corresponded to Al–OH vibration [26,36,37], while a band at around 1064 cm^{-1} was related to CO_3^{2-} symmetric stretching vibration [26,37]. Both of these bands are characteristic of brucite-like structures and were in agreement with the literature [26,36–38]. Modes related to the presence of nitroprusside anions were observed in the frequency range from 2000 to 2200 cm^{-1}. According to theoretical group calculations for the $[Fe(CN)_5NO]^{2-}$ anion, strong modes would be expected at around 2066, 2103, and 2136 cm^{-1}, related

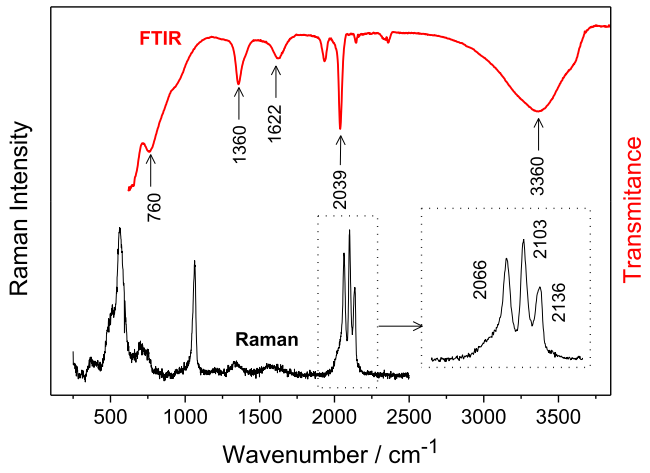

Fig. 3. FTIR and Raman spectra of LDH-NP. The positions of the main bands are indicated, for better visualization. The inset in the Raman spectrum shows the modes related to C—N equatorial and axial vibrations.

to C—N equatorial and axial vibrations. For better visualization, these bands are highlighted in the inset of Fig. 3, from which it can be seen that the most intense band was the second band corresponding to C—N equatorial stretching. The Raman spectrum also showed low frequency modes at around 364 cm^{-1} and 496 cm^{-1}, related to Fe—C—N equatorial bending and Fe–C axial stretching, respectively.

The thermogravimetric analysis and derivative curves for LDH-NP, shown in Fig. 4, revealed three stages of thermal decomposition. The first, from room temperature to 171 °C, corresponded to the release of adsorbed and interlamellar water molecules [26,36], with a mass loss of 20.5%. This release enabled determination of the number of water units present in the interlayers, with a calculated value of 7.3. The second stage of decomposition was the removal of hydroxyl ions [26,36] at around 279 °C, with a mass loss of 11.9%. The last stage, at around 371 °C, was related to decomposition of the intercalated anions [26,36,39,40], with a mass loss of 16.7%.

3.2. Removal of As using LDH and LDH-NP

Fig. 5 shows the removal percentages of the As(III), As(V), and DMA species by LDH and LDH-NP, at different pH values.

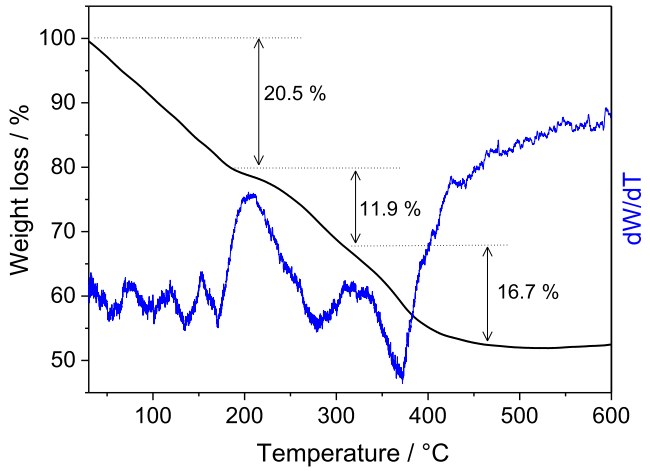

Fig. 4. Thermogravimetric analysis curves for LDH-NP: TGA (black line) and DTG (blue line). (For interpretation of the references to colour in this figure legend, the reader is referred to the web version of this article.)

LDH presented high removal capacity for the As(V) species, under all the conditions investigated (101.07% removal at pH 2.00, 89.40% removal at pH 6.02, and 47.31% removal at pH 12.00), while low removal of the As(III) species was observed at pH 6.02 (7.93% removal). For these same species at the same pH values, the extraction percentages increased when LDH was replaced by LDH-NP, which also showed capacity for the adsorption of DMA at pH 2.00 (25.10% removal) and As(III) at pH 12.00 (60.83% removal). These results indicated that both materials (LDH and LDH-NP) were able to selectively adsorb one or another species of arsenic, which would enable their use in speciation studies. Notably, As(V) could be selectively adsorbed at pH 2.00 or 12.00, using LDH. On the other hand, at pH 2.00, LDH-NP could be used to adsorb DMA and As(V), but not As(III), while at pH 6.02 and 12.00, it could be used to adsorb only the inorganic As (III) and As(V) species. Since arsenic is most commonly found as an oxyanion in inorganic compounds in the forms of As(III) (arsenite, AsO_3^{3-}) and As(V) (arsenate, AsO_4^{3-}), and since the inorganic forms, especially As(III), are more toxic than the organic forms, the characteristics of adsorption of the different arsenic species on LDH-NP indicate the potential of this material to provide their speciation. Given these observations, isotherm studies were performed for adsorption of the As(III), As(V), and DMA species on LDH-NP.

3.3. Adsorption isotherms for the removal of different As species on LDH-NP

Fig. 6 shows the adsorption isotherms for removal of the As(III), As(V), and DMA species on LDH-NP, at 25 °C. The corresponding extraction percentages are shown in Fig. S1 (Supplementary Material).

In general, the adsorption isotherm profiles showed strong dependence on the adsorbed arsenic species and the pH of the medium. At pH 2.00 (Fig. 6a), only the As(V) species was adsorbed in a large extension, with a rapid increase of q_e as C_e increased to around 40 mg L^{-1}, after which q_e became constant at around 76.9 mg g^{-1}, indicating saturation of the adsorbent surface. Under the conditions evaluated, almost all the As(V) was removed from the solution, with extraction percentages varying between 103.8% and 87.7% (Fig. S1).

When the pH was changed from 2.00 to 6.02 (Fig. 6b), the amount of As(V) adsorbed decreased markedly, with maximum

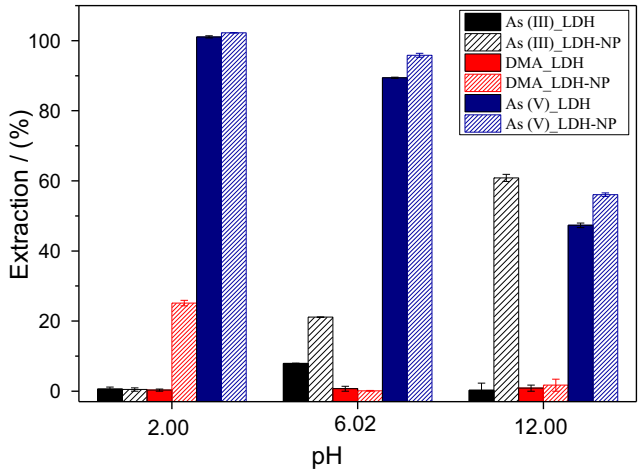

Fig. 5. Percentage extraction of As(III), As(V), and DMA, using LDH and LDH-NP, at different pH values. Conditions: 25 °C, 150 rpm, contact time of 24 h, initial As concentration of 10 mg L^{-1}, and adsorbent concentration of 1.33 g L^{-1}. The pH values reported are the values measured in pH meter, respecting the significative digits.

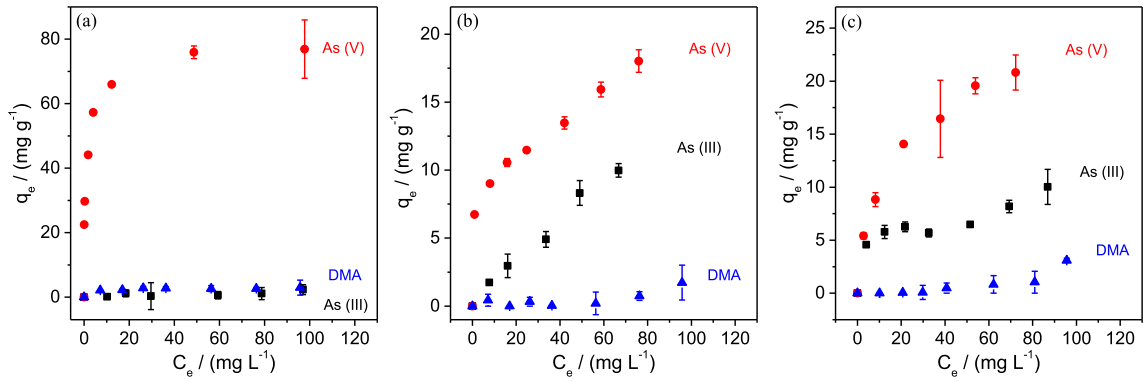

Fig. 6. Isotherms for adsorption of As(III) (■), As(V) (●), and DMA (▲) on LDH-NP at (a) pH 2.00, (b) pH 6.02, and (c) pH 12.00. Conditions: 25 °C, 150 rpm, contact time of 24 h, and adsorbent concentration of 1.33 g L^{-1}.

Table 2
Parameters of the Langmuir and Freundlich isotherm models for the adsorption of different arsenic species on LDH-NP. Conditions: 25 °C, 150 rpm, contact time of 24 h, and adsorbent concentration of 1.33 g L^{-1}.

Species	Model	Parameters	pH 2.00	pH 6.02	pH 12.00
As (V)	Langmuir	$q_{máx}$ (mg g^{-1})	77.63	18.84	24.15
		K_L (L mg^{-1})	0.92	0.10	0.07
		R^2	0.9996	0.9501	0.9866
	Freundlich	K_F	1	6.1476	3.6089
		n	5.8082	4.5446	2.3752
		R^2	0.9609	0.9215	0.9912
As (III)	Langmuir	$q_{máx}$ (mg g^{-1})	–	31.91	10.11
		K_L (L mg^{-1})	–	0.0066	0.07
		R^2	–	0.4464	0.8774
	Freundlich	K_F	–	0.31	3.26
		n	–	1.2172	4.7776
		R^2	–	0.9825	0.7253

*Fitting was not performed for the adsorption of DMA or for the adsorption of As(III) at pH 2.00, because the adsorptions were very low.

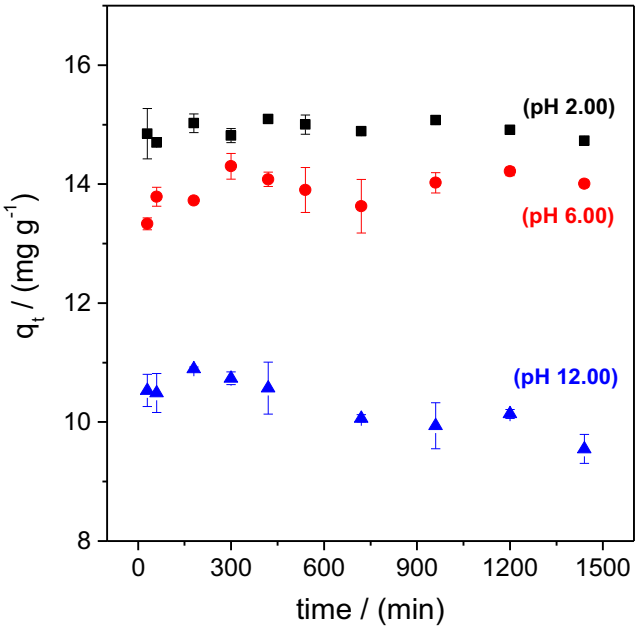

Fig. 7. Adsorption of As(V) on LDH-NP, as a function of time, at different pH values. Conditions: 25 °C, 150 rpm, initial adsorbate concentration of 20 mg L^{-1}, and adsorbent concentration of 1.33 mg L^{-1}.

q_e of 18.0 mg g^{-1} when the equilibrium concentration was 75.8 mg L^{-1}. This decrease of q_e was accompanied by a change in the adsorption isotherm profile, which exhibited a continuous increase

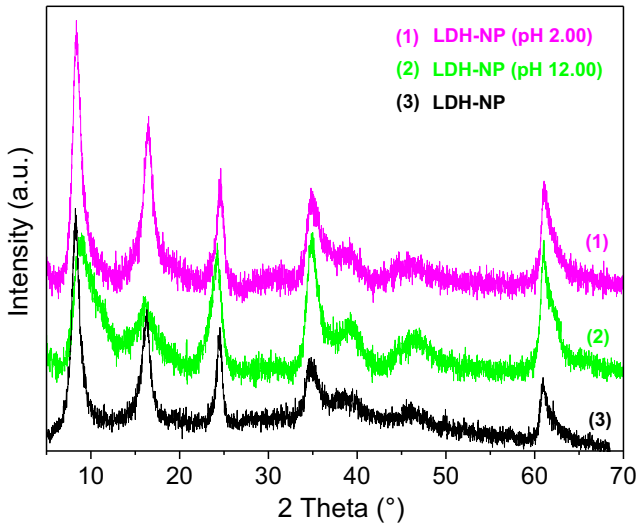

Fig. 8. XRD patterns for LDH-NP before (black line) and after the adsorption of As (V) in an acidic medium (pH 2.00, magenta line) and a basic medium (pH 12.00, green line). (For interpretation of the references to colour in this figure legend, the reader is referred to the web version of this article.)

of q_e as C_e increased, within the range investigated. In addition, there was the adsorption of a small amount of As(III), with a linear increase of q_e as C_e increased.

Finally, at pH 12.00 (Fig. 6c), the amounts of As(III) and As(V) adsorbed were similar to those obtained at pH 6.02. There was a marked change in the isotherm for As(III), with the LDH-NP surface

becoming saturated at very low concentrations of the adsorbate. The maximum q_e values obtained for As(V) and As(III) were 20.8 and 10.00 mg g^{-1}, respectively.

The results obtained for the adsorption of As(V) were similar to those reported by Guo et al. [24], who found that higher pH caused a decrease of the amount of As(V) adsorbed on LDH of the type CuMgFeLa-LDH, which was attributed to increased electrostatic repulsion between the As(V) species and the LDH surface. Similar results and explanation were presented by Hongtao et al. [21] for the adsorption of As(V) on LDH of the type MgAlFe-LDH with intercalated chloride or nitrate anions.

However, it should be noted that the highest q_e values for As(V) were obtained at pH 2.00, at which some of the As(V) species were in the neutral form (Equation (4)). At the same time, the adsorption of As(III) increased when the pH was increased from 2.00, at which the species were in the neutral form, to 6.02 or 12.00, at which they

Table 3
Lattice parameters, basal spacings, and crystallite sizes for the LDH-NP saturated with As(V).

Samples	Interplanar distance (Å)			Basal spacing (Å)	Lattice parameter (Å)		Crystallite size (nm)
	d_{003}	d_{006}	d_{009}		a	c	
LDH-NP (pH 2.00)	10.56	5.37	3.61	6.51	3.04	32.13	6
LDH-NP (pH 12.00)	9.92	5.50	3.67	6.36	3.04	31.93	5

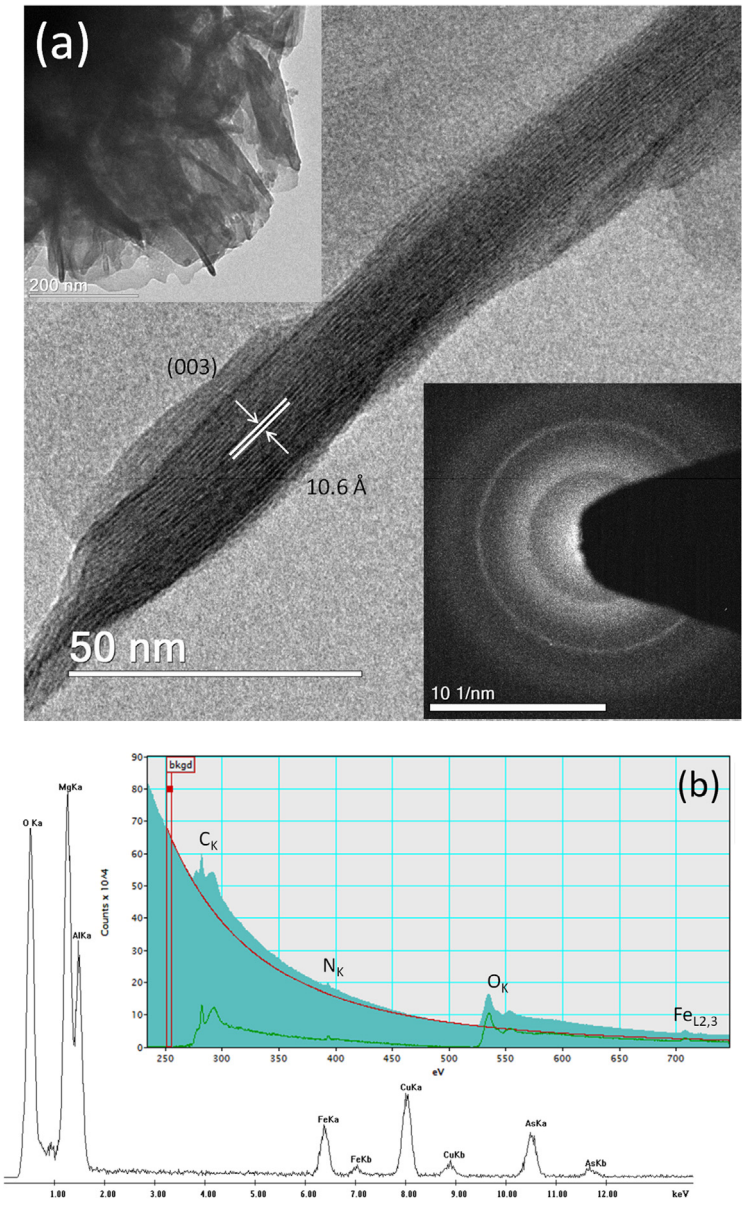

Fig. 9. (a) High-resolution TEM image for the LDH-NP materials saturated with As(V) at pH = 2.00, showing interplanar spacings of 10.6 Å, corresponding to the (0 0 3) planes of the rhombohedral ($R\bar{3}m$) structure. Inset: low-magnification TEM image (top left) and SAED pattern (bottom right) for the polycrystalline LDH-NP sample; (b) EDS/EELS spectra showing the electronic energies of the ions present. Note the signals from As ions (K_a and K_b) observed in the EDS spectrum.

were neutral or positively charged, respectively (Equation (5)). Finally, no adsorption of the DMA species was observed at pH 6.02, at which they were partially negatively charged (Equation (6)) and the LDH-NP was positively charged (pH_{pzc} equal to 8.30; Fig. S2, Supplementary Material). Hence, the adsorption of the arsenic species on LDH-NP was not only due to electrostatic attraction, but could also have involved specific interactions between the arsenic species and the nitroprusside incorporated in the LDH.

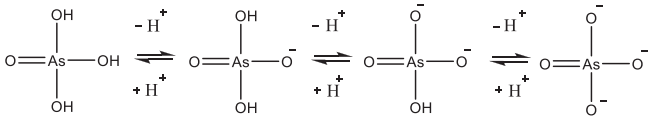

(4)

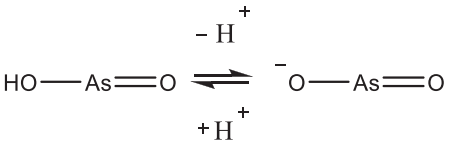

(5)

pK$_a$ = 9.3

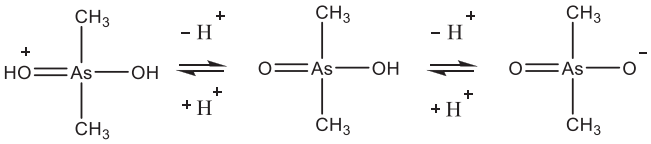

(6)

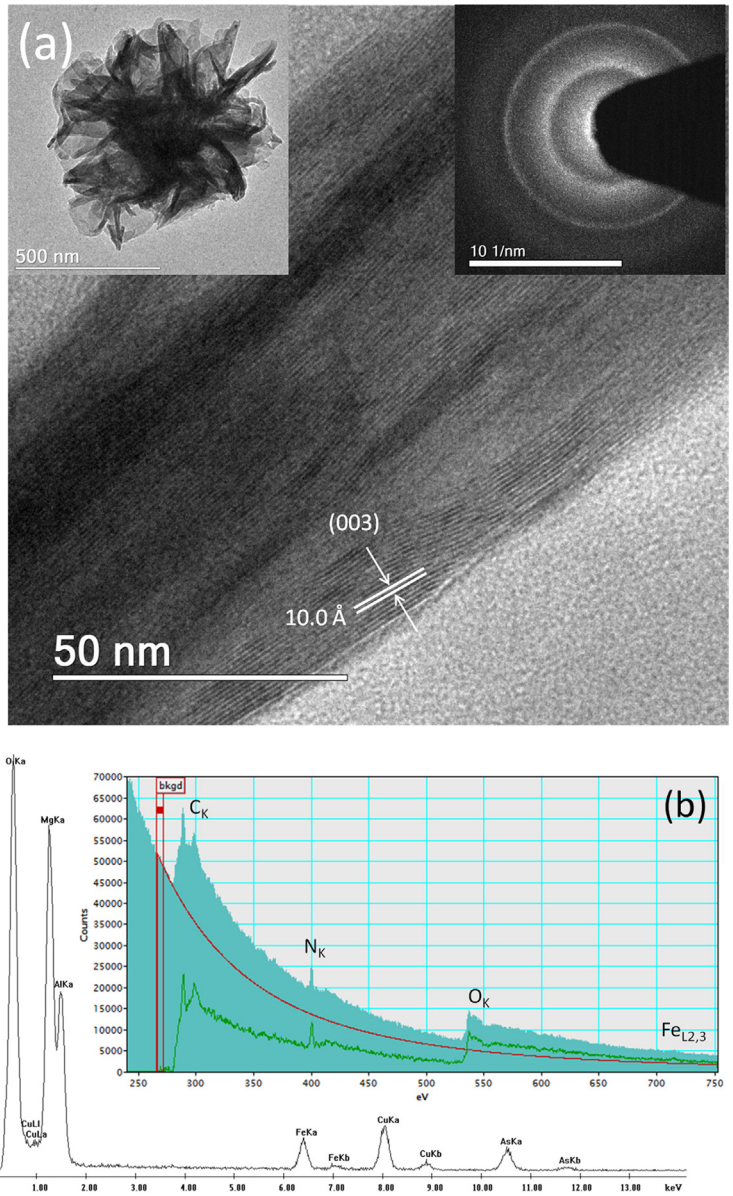

Fig. 10. (a) High-resolution image for the LDH-NP materials saturated with As(V) at pH = 12.00, showing interplanar spacings of 10.0 Å related to the (0 0 3) planes. Inset: low-magnification TEM image (top left) and SAED pattern (top right) evidencing the polycrystalline nature of the LDH-NP sample; (b) EDS/EELS spectra with the electronic energies of the ions clearly identified. The signals from the As(V) ions (K_a and K_b) can be observed in the EDS spectrum.

Table 2 shows the parameters for fitting of the Langmuir and Freundlich isotherm models to the experimental adsorption data. The fits are shown in Fig. S3 (Supplementary Material).

For the adsorption of As(V) on LDH-NP at pH 2.00 and 6.02, the Langmuir model provided the best fit to the experimental data with R^2 values equals to 0.9996 and 0.9501, respectively. The maximum adsorption capacities (q_{max}) (77.63 and 18.84 mg g^{-1}) are in agreement with the values obtained experimentally (76.9 and 18.0 mg g^{-1}), respectively. On the other hand, at pH 12.00, the best fit was obtained using the Freundlich model, with R^2 values of 0.9912. For the adsorption of As(III), the Freundlich and Langmuir models provided the best fits to the experimental data obtained at pH 6.02 and 12.0, respectively. These results suggested that the features of the adsorption process were dependent on both the pH of the medium and the arsenic species.

Fig. 7 shows the amount of As(V) adsorbed (q_t) as a function of time, for different pH values. The process presented rapid kinetics, with the value of q_t becoming practically constant after 30 min.

3.4. Characterization of LDH-NP saturated with As(V)

Characterization was performed of LDH-NP once it had been saturated with As(V). Fig. 8 shows XRD data of LDH-NP after adsorption of As(V) at pH 2.00 and 12.00, as well as of pure LDH-NP, in order to compare the structures of the materials before and after the adsorption. It can be seen that the adsorption of As (V) did not alter the structure of the material, since the samples exhibited the same diffraction pattern. The interplanar distances for LDH-NP saturated with As(V) at pH 2.00 were 10.56, 5.37, and 3.61 Å for d_{003}, d_{006}, and d_{009}, respectively. The calculated basal spacing was 6.51 Å and the crystallite size was 6 nm. For LDH-NP saturated with As(V) at pH 12.00, the values obtained for the interplanar distances were d_{003} = 9.92 Å, d_{006} = 5.50 Å, and d_{009} = 3.67 Å, resulting in basal spacing of 6.36 Å and crystallite size of 5 nm. The basal spacing remained almost unchanged after the adsorption of As(V), suggesting that arsenic did not replace the nitroprusside in the LDH structure (see Table 3), but it interacted with the anionic complex.

The LDH-NP samples saturated with As(V) were also investigated by TEM, and the results are displayed in Figs. 9 and 10. Morphologies and chemical/structural features of the LDH-NP materials saturated at pH = 2.00 and pH = 12.00 were examined. Fig. 9 presents TEM/SAED images (Fig. 9a), and EDS/EELS spectra (Fig. 9b) obtained for the LDH-NP materials saturated at pH = 2.00. The morphology of the samples shows also nanometer-sized platelets (Fig. 9a, inset: top left), while high-resolution TEM image (Fig. 9) shows well-defined interplanar spacings of the order of 10.6 Å, which are related to the (0 0 3) planes, in agreement with the results from XRD (Table 1). The polycrystalline character of these LDH-NP materials (pH = 2.00) could be verified (SAED pattern, Fig. 9a, inset: bottom right), where diffuse rings are present. Fig. 9b presents the EDS/EELS data with many spectral features corresponding to different excitation processes. EDS spectrum showed the presence of As(V) ions, as expected for the samples treated at pH = 2.00. Fig. 10 shows the results of the TEM characterization for the samples saturated at pH = 12.00. Again, polycrystalline, nanometer-sized platelets could be observed (see inset, top images), with interplanar spacing of about 10.0 Å, which is in agreement with the XRD data (Table 1). As(V) ions were easily detected in these LDH-NP samples by EDS (Fig. 10b), as expected for these saturated materials at pH = 12.00.

Fig. 11 shows the FTIR (Fig. 11a) and Raman (Fig. 11b) spectra for LHD-NP saturated with As(V). The bands in the FTIR spectra were practically the same for all the samples analyzed, indicating that there was no structural change of the LDH after the incorporation of As(V). However, a band at around 1932 cm^{-1} in the spectra for pure LDH-NP (Fig. 3) and LDH-NP saturated with As(V) at pH 12.00 was not observed when the material was saturated with As (V) at pH 2.00. This band at around 1932 cm^{-1} was related to NO stretching, so the results suggested that the acidic medium favored the release of the nitric oxide ligand from the complex during intercalation [23,29]. It is known that nitroprusside decomposes to produce ferrocyanide and nitrosyl groups, following insertion into LDH [29]. Hence, the presence of $[Fe(CN)_5H_2O]^{3-}$ was predominant in the interlamellar domain of LDH-NP at pH 2.00. On the other hand, for LDH-NP and LDH-NP loaded with As(V) at pH 12.00, the spectra showed the presence of bands related to NO stretching, suggesting the coexistence of $[Fe(CN)_5NO]^{2-}$ and $[Fe(CN)_5H_2O]^{3-}$ in the interlamellar domain of MgAl-LDH [23]. Finally, the Raman spectra for the pure material and the materials saturated with As(V) were very similar, corroborating the XRD and FTIR results indicating that the adsorption did not cause structural changes in the material. There was only a slight difference in the region from 2000 to 2200 cm^{-1}, with the presence of the arsenic species in the structure of the material resulting in the absence of the third vibrational mode corresponding to the equatorial and axial vibration of C—N, at approximately 2136 cm^{-1}. Therefore, it was likely that the presence of As(V) inhibited this vibrational mode, characteristic of the $[Fe(CN)_5NO]^{2-}$ anion.

3.5. Comparison with literature data

Table 4 presents a list of different adsorbents that have been used to remove As(V) from aqueous solutions. Comparison among the materials shows that LDH-NP present a good performance, because its adsorption capacity (q_{max}) is between the maximum and minimum values reported in the literature for other LDHs. In addition, this value is comparable to most of other conventional materials such as hydrogels and cellulose derivatives.

4. Conclusions

The LDH of the type MgAl-LDH with incorporated nitroprusside as an adsorbent was applied for the removal of different species of arsenic from aqueous solutions. For the first time, the adsorption of organic arsenic on LDH was evaluated. The incorporation of nitroprusside in the LDH affected the adsorption characteristics of the material, leading to increases of the extraction percentages for

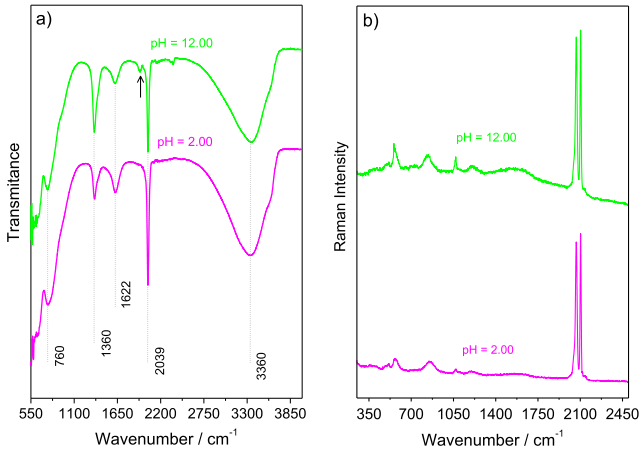

Fig. 11. (a) FTIR and (b) Raman spectra of LDH-NP after As(V) adsorption. The green and magenta lines represent the results obtained for pH 12.00 and 2.00, respectively. The positions of the main FTIR bands are indicated, for better visualization. (For interpretation of the references to colour in this figure legend, the reader is referred to the web version of this article.)

Table 4
Comparison among different adsorbent materials for removal of As(V) from aqueous solutions.

Adsorbent	q_{max} (mg g^{-1})	T (°C)	pH	Equilibrium time (min)	Reference
MgAl-LDH-NP	77.63	25	2.00	30	This study
Calcinated MgAl-LDH	102.9	25	3.00	360	[2]
CuMgFeLa-LDH	25.6–43.5	25	6.00	480	[24]
La(III)-montmorillonite Hydrogel beads	58.75	25	4.00	240	[41]
CoFeAl-LDH@Fe_3O_4@PA	167	25	6.00	5	[42]
Magnetite-loaded amino modified nanocellulose	85.3	25	6.00	90	[43]
Magnetite-loaded amino modified microcellulose	18.5	25	6.00	60	[43]

inorganic arsenic species, at all the pH values studied. The amounts of arsenic adsorbed varied according to the initial pH of the solution and the chemical nature of the arsenic species, indicating that the adsorption process was governed by electrostatic forces and specific interactions between the arsenic species and the nitroprusside incorporated in the LDH. In addition, the features of the adsorption process depended on the pH of the medium and the arsenic species as suggested by the analysis of the Langmuir and Freundlich isotherm models. Finally, the antagonistic behaviors of adsorption for the different arsenic species in the different conditions studied indicated the possibility of the material being used to selectively remove DMA, As(III), and/or As(V) under specific conditions, making this material a potential adsorbent for the treatment of water contaminated with arsenic or for the arsenic speciation.

CRediT authorship contribution statement

Gabriella Alexandre Borges: Investigation, Formal analysis, Visualization, Writing - original draft. **Gabriel Max Dias Ferreira:** Conceptualization, Methodology, Writing - review & editing. **Kisla Prislen Félix Siqueira:** Methodology, Visualization, Writing - original draft. **Anderson Dias:** Methodology, Visualization, Writing - original draft. **Keirom Osmany Nàjera Navarro:** Investigation. **Silvia Juliana Barros e Silva:** Investigation. **Guilherme Dias Rodrigues:** Validation, Methodology. **Aparecida Barbosa Mageste:** Resources, Project administration, Conceptualization.

Declaration of Competing Interest

The authors declare that they have no known competing financial interests or personal relationships that could have appeared to influence the work reported in this paper.

Acknowledgements

The authors are grateful to Fundação de Amparo à Pesquisa do Estado de Minas Gerais (FAPEMIG, grants APQ-03210-15 and APQ-00540-17), Conselho Nacional de Desenvolvimento Científico e Tecnológico (CNPq, grant 309668/2019-0), Coordenação de Aperfeiçoamento de Pessoal de Nível Superior (CAPES, Finance Code 001), Universidade Federal de Ouro Preto (UFOP, grant 23109.004080/2019-88), Universidade Federal de Minas Gerais (UFMG), and Instituto Federal de Minas Gerais Campus Ouro Preto (IFMG – OP) for financial support and scholarships. The Center of Microscopy at the Universidade Federal de Minas Gerais (http://www.microscopia.ufmg.br) is also acknowledged for providing the equipment and technical support for experiments involving electron microscopy. Thanks are also due to the Laboratório de Biohidrometalurgia e Tratamento de Efluentes (UFOP) for conducting the analysis using ICP-OES.

Appendix A. Supplementary material

Supplementary data to this article can be found online at https://doi.org/10.1016/j.jcis.2020.04.078.

References

[1] S. Islam, M.M. Rahman, M.A. Rahman, R. Naidu, Inorganic arsenic in rice and rice-based diets: health risk assessment, Food Control 82 (2017) 196–202, https://doi.org/10.1016/j.foodcont.2017.06.030.
[2] S.H. Lee, M. Tanaka, Y. Takahashi, K.W. Kim, Enhanced adsorption of arsenate and antimonate by calcined Mg/Al layered double hydroxide: Investigation of comparative adsorption mechanism by surface characterization, Chemosphere 211 (2018) 903–911, https://doi.org/10.1016/j.chemosphere.2018.07.153.
[3] R. Mukhopadhyay, K.M. Manjaiah, S.C. Datta, B. Sarkar, Comparison of properties and aquatic arsenic removal potentials of organically modified smectite adsorbents, J. Hazard. Mater. 377 (2019) 124–131, https://doi.org/10.1016/j.jhazmat.2019.05.053.
[4] P. Maziarz, J. Matusika, T. Strączekb, C. Kapustab, W.M. Wochb, W. Tokarzb, A. Radziszewskac, T. Leiviskä, Highly effective magnet-responsive LDH-Fe oxide composite adsorbents for As(V) removal, Chem. Eng. J. 362 (2019) 207–216, https://doi.org/10.1016/j.cej.2019.01.017.
[5] H. Uppal, S. Chawla, A.G. Joshi, D. Haranath, N. Vijayan, N. Singh, Facile chemical synthesis and novel application of zinc oxysulfide nanomaterial for instant and superior adsorption of arsenic from water, J. Clean. Prod. 208 (2019) 458–469, https://doi.org/10.1016/j.jclepro.2018.10.023.
[6] F. González-Martínez, D. Sánchez-Rodas, D.D. Cáceres, M.F. Martínez, L.A. Quiñonese, B. Johnson-Restrepo, Arsenic exposure, profiles of urinary arsenic species, and polymorphism effects of glutathione-s-transferase and metallothioneins, Chemosphere 212 (2018) 927–936, https://doi.org/10.1016/j.chemosphere.2018.08.139.
[7] A.E. Burakov, E.V. Galunin, I.V. Burakova, A.E. Kucherova, S. Agarwal, A.G. Tkachev, V.K. Gupta, Adsorption of heavy metals on conventional and nanostructured materials for wastewater treatment purposes: a review, Ecotoxicol. Environ. Saf. 148 (2018) 702–712, https://doi.org/10.1016/j.ecoenv.2017.11.034.
[8] C.B. Godiya, Y. Xiao, X. Lu, Amine functionalized sodium alginate hydrogel for efficient and rapid removal of methyl blue in water, Int. J. Biol. Macromol. 144 (2020) 671–681, https://doi.org/10.1016/j.ijbiomac.2019.12.139.
[9] A.R. Hernandez-Martínez, J.A. Lujan-Montelongo, C. Silva-Cuevas, J.D. Mota-Morales, M. Cortez-Valadez, A.J. Ruíz-Baltazar, M. Cruz, J. Herrera-Ordonez, Swelling and methylene blue adsorption of poly(N, N-dimethylacrylamide-co-2-hydroxyethyl methacrylate) hydrogel, React. Funct. Polym. 122 (2018) 75–84, https://doi.org/10.1016/j.reactfunctpolym.2017.11.008.
[10] J. Mohanraj, D. Durgalakshmi, S. Balakumar, P. Aruna, S. Ganesan, Saravanan Rajendran, Mu. Naushad, Low cost and quick time absorption of organic dye pollutants under ambient condition using partially exfoliated graphite, J. Water Process Eng. 34 (2020) 101078–101085, https://doi.org/10.1016/j.jwpe.2019.101078.
[11] A.L. Ramos-Jacques, J.A. Lujan-Montelongo, C. Silva-Cuevas, M. Cortez-Valadez, M. Estevez, A.R. Hernandez-Martínez, Lead (II) removal by poly(N, N-dimethylacrylamide-co-2-hydroxyethyl methacrylate), Eur. Polym. J. 101 (2018) 262–272, https://doi.org/10.1016/j.eurpolymj.2018.02.032.
[12] Y. Yue, X. Wang, Q. Wu, J. Han, J. Jiang, Highly recyclable and super-tough hydrogel mediated by dual-functional TiO_2 nanoparticles toward efficient photodegradation of organic water pollutants, J. Colloid Interface Sci. 564 (2020) 99–112, https://doi.org/10.1016/j.jcis.2019.12.069.
[13] Z.A. Bhatti, K. Qureshi, G. Maitlo, S. Ahmed, Study of PAN fiber and iron ore adsorbents for arsenic removal, Civil Eng. 6 (2020) 548–562. https://doi.org/10.28991/cej-2020-03091491.
[14] X. Guo, F. Chen, Removal of arsenic by bead cellulose loaded with iron oxyhydroxide from groundwater, Environ. Sci. Technol. 39 (2005) 6808–6818, https://doi.org/10.1021/es048080k.
[15] X. Guo, Y. Du, F. Chen, H. Park, Y. Xie, Mechanism of removal of arsenic by bead cellulose loaded with iron oxyhydroxide (β-FeOOH): EXAFS study, J. Colloid Interface Sci. 314 (2007) 427–433, https://doi.org/10.1016/j.jcis.2007.05.071.
[16] S.Y. Lee, K.W. Jung, J.W. Choi, Y.J. Lee, In situ synthesis of hierarchical cobalt-aluminum layered double hydroxide on boehmite surface for efficient removal of arsenate from aqueous solutions: Effects of solution chemistry factors and

sorption mechanis, Chem. Eng. J. 368 (2019) 914–923, https://doi.org/10.1016/j.cej.2019.03.043.
[17] D. Santra, R. Ghosh, M. Das, P. Majumdar, M. Sarkar, Adsorption of arsenic(V) onto metal loaded cellulose nanocomposite bead (mcnb)-isotherm and thermodynamic study, Eur. Chem. Bull. 3 (2014) 692–698. https://doi.org/10.17628/ECB.2014.3.692.
[18] J. Wang, T. Zhang, M. Li, Y. Yang, P. Lu, P. Ning, Q. Wang, Arsenic removal from water/wastewater using layered double hydroxide derived adsorbents, a critical review, RSC Adv. 8 (2018) 22694–22709, https://doi.org/10.1039/c8ra03647k.
[19] H. Asiabi, Y. Yamini, M. Shamsayei, Highly selective and efficient removal of arsenic(V), chromium(VI) and selenium(VI) oxyanions by layered double hydroxide intercalated with zwitterionic glycine, J. Hazard. Mater. 339 (2017) 239–247, https://doi.org/10.1016/j.jhazmat.2017.06.042.
[20] K. Goh, T. Lima, Z. Dong, Application of layered double hydroxides for removal of oxyanions: a review, Water Res. 42 (2008) 1343–1368, https://doi.org/10.1016/j.watres.2007.10.043.
[21] L. Hongtao, L. Shuxia, Z. Hua, O. Yanling, Y. Daqiang, Z. Jianfua, Z. Zhiliang, Comparative study on synchronous adsorption of arsenate and fluoride in aqueous solution onto MgAlFe-LDHs with different intercalating anions, RSC Adv. (2018), https://doi.org/10.1039/c8ra05968c.
[22] G.P. Gillman, A simple technology for arsenic removal from drinking water using hydrotalcite, Sci. Total Environ. 366 (2006) 926–993, https://doi.org/10.1016/j.scitotenv.2006.01.036.
[23] L.F. da Silva, J. Tronto, H.P. Oliveira, J.B. Valim, Intercalation and electrochemical studies of nitroprusside anion into Zn-Al layered double hydroxide, J. Incl. Phenom. Macrocycl. Chem. 46 (2003) 187–193, https://doi.org/10.1023/A:1026370917291.
[24] Y. Guo, Z. Zhua, Y. Qiub, J. Zhao, Adsorption of arsenate on Cu/Mg/Fe/La layered double hydroxide from aqueous solutions, J. Hazard. Mater. 239 (2012) 279–288, https://doi.org/10.1016/j.jhazmat.2012.08.075.
[25] T. Türk, I. Alp, H. Deveci, Adsorption of As(V) from water using Mg–Fe-based hydrotalcite (FeHT), J. Hazard. Mater. 171 (2009) 665–670, https://doi.org/10.1016/j.jhazmat.2009.06.052.
[26] M.A. Teixeira, A.B. Mageste, A. Dias, L.S. Virtuoso, K.P.F. Siqueira, Layered double hydroxides for remediation of industrial waster containing manganese and fluoride, J. Clean. Prod. 171 (2018) 275–284, https://doi.org/10.1016/j.jclepro.2017.10.010.
[27] W. Hayes, R. Loudon, Scattering of Light by Crystals, Wiley, New York, 1978.
[28] S. Periyasamy, V. Gopalakannan, N. Viswanathan, Hydrothermal assisted magnetic nano-hydroxyapatite encapsulated alginate beads for efficient Cr(VI) uptake from water, J. Environ. Chem. Eng. 6 (2018) 1443–1454, https://doi.org/10.1016/j.jece.2018.01.007.
[29] J.W. Boclair, P.S. Braterman, B.D. Brister, F. Yarberry, Layer-anion interactions in magnesium aluminum layered double hydroxides intercalated with cobalticyanide and nitroprusside, Chem. Mater. 11 (1999) 2199–2204. https://doi-org.ez27.periodicos.capes.gov.br/10.1021/cm990148l.
[30] M.V. Bukhtiyarova, A rewiew on effect of synthesis conditions on the formation of layered double hydroxides, J. Solid State Chem. 269 (2019) 494–506, https://doi.org/10.1016/j.jssc.2018.10.018.
[31] J. Pérez-Ramírez, G. Mul, F. Kapteijn, J.A. Moulijn, In situ investigation of the thermal decomposition of Co-Al hydrotalcite in different atmospheres, J. Mater. Chem. 11 (2001) 821–830, https://doi.org/10.1039/b009320n.
[32] J.C. Taylor, M.H. Mueller, R.L. Hitterman, A neutron diffraction study of ferroelectric, KFCT, K4Fe(CN)6.3D2O, above the curie temperature, Acta Cryst. A26 (1970) 559–567, https://doi.org/10.1107/S0567739470001407.
[33] P.P. Ghalsasi, P.S. Ghalsasi, D.V.S. Muthu, Back-bonding signature with high pressure: Raman studies on silver nitroprusside, Inorg. Chem. 56 (2017) 9669–9675, https://doi.org/10.1021/acs.inorgchem.7b01151.
[34] M. Bellotto, B. Rebours, O. Clause, J. Lynch, D. Bazin, E. Elkaim, A reexamination of hydrotalcite crystal cehmistry, J. Phys. Chem. 100 (1996) 8527–8534, https://doi.org/10.1021/jp960039j.
[35] M.C. Richardson, P.S. Braterman, Infrared spectra of oriented and nonoriented layered doulbe hydroxides in the range from 4000 to 250 cm^{-1}, with evidence for regular short-range order in a synthetic magnesium-aluminum LDH with Mg: Al = 2:1 but not with Mg: Al = 3:1, J. Phys. Chem. C 111 (2007) 4209–4215. https://doi-org.ez27.periodicos.capes.gov.br/10.1021/jp064744w.
[36] A.C. Vieira, R.L. Moreira, A. Dias, Raman scattering and fourier transform infrared spectroscopy of $Me_6Al_2(OH)_{16}Cl_2.4H_2O$ (Me = Mg, Ni, Zn, Co and Mn) and $Ca_2Al(OH)_6Cl.2H_2O$ hydrotalcites, J. Phys. Chem. C 113 (2009) 13358–13368, https://doi.org/10.1021/jp902566r.
[37] J. Pérez-Ramírez, G. Mul, J.A. Molijn, In situ Fourier transform infrared and laser Raman spectroscopic study of the thermal decomposition of Co-Al and Ni-Al hydrotalcites, Vibration. Spec. 27 (2001) 75–88, https://doi.org/10.1016/S0924-2031(01)00119-9.
[38] A.D. Santo, H. Osiry, E. Reguera, P. Alborés, R.E. Carbonio, A.B. Altabef, D.M. Gil, New coordination polymers based on 2-methylimidazole and transition metal nitroprusside containing building blocks: synthesis, structure and magnetic properties, New J. Chem. 42 (2018) 1347–1355, https://doi.org/10.1039/C7NJ03585C.
[39] D. Cosano, C. Esquinas, C.J. Sanchidrián, J.R. Ruiz, Use of Raman spectroscopy to assess the efficiency of MgAL mixed oxides in removing cyanide from aqueous solutions, Appl. Surf. Sci. 364 (2016) 428–433, https://doi.org/10.1016/j.apsusc.2015.12.181.
[40] M.A. Aramendía, Y. Avilés, V. Borau, J.M. Luque, J.M. Marinas, J.R. Ruiz, F.J. Urbano, Thermal decomposition of Mg/Al and Mg/Ga layered-double hydroxides: a spectroscopic study, J. Mater. Chem. 9 (1999) 1603–1607. https://doi-org.ez27.periodicos.capes.gov.br/10.1039/A900535H.
[41] S. Yan, Q. An, L. Xia, S. Liu, S. Song, J.R. Rangel-Méndeze, As(V) removal from water using the La(III) – montmorillonite hydrogel beads, React. Funct. Polym. 147 (2020) 1–9, https://doi.org/10.1016/j.reactfunctpolym.2019.104456.
[42] L. Adlnasab, N. Djafarzadeh, A. Maghsodi, A new magnetic bio-sorbent for arsenate removal from the contaminated water: characterization, isotherms, and kinetics, Environ. Health Eng. Manage. J. 7 (2020) 49–58. https://doi.org/10.34172/EHEM.2020.07.
[43] K. Taleb, J. Markovski, Z. Velickovic, J. Rusmirovic, M. Rancic, V. Pavlovic, A. Marinkovic, Arsenic removal by magnetite-loaded amino modified nano/microcellulose adsorbents: effect of functionalization and media size, Arab. J. Chem. 12 (2019) 4675–4693, https://doi.org/10.1016/j.arabjc.2016.08.006.